

MaxSAT decoders for arbitrary CSS codes

Mohammadreza Noormandipour^{1,2,*} and Tobias Haug^{3,†}

¹*TCM Group, Cavendish Laboratory, Department of Physics,
J J Thomson Avenue, Cambridge CB3 0HE, United Kingdom*

²*Artificial Intelligence Research Lab, Nokia Bell Labs; Broers Building, 21 J.J. Thomson Avenue, Cambridge, CB3 0FA, UK*

³*Quantum Research Center, Technology Innovation Institute, Abu Dhabi, UAE*

(Dated: October 3, 2024)

Quantum error correction (QEC) is essential for operating quantum computers in the presence of noise. Here, we accurately decode arbitrary Calderbank-Shor-Steane (CSS) codes via the maximum satisfiability (MaxSAT) problem. We show how to map quantum maximum likelihood problem of CSS codes of arbitrary geometry and parity check weight into MaxSAT problems. We incorporate the syndrome measurements as hard clauses, while qubit and measurement error probabilities, including biased and non-uniform, are encoded as soft MaxSAT clauses. For the code capacity of color codes on a hexagonal lattice, our decoder has a higher threshold and superior scaling in noise suppression compared to belief propagation with ordered statistics post-processing (BP-OSD), while showing similar scaling in computational cost. Further, we decode surface codes and recently proposed bivariate quantum low-density parity check (QLDPC) codes where we find lower error rates than BP-OSD. Finally, we connect the complexity of MaxSAT decoding to a computational phase transition controlled by the clause density of the MaxSAT problem, where we show that our mapping is always in the computationally “easy” phase. Our MaxSAT decoder can be further parallelised and implemented on ASICs and FPGAs, promising further substantial speedups. Our work provides a flexible platform towards practical applications on quantum computers.

I. INTRODUCTION

Quantum computers promise to solve important problems that cannot be addressed by classical computers [1–3]. To run quantum computers even in the presence of noise, quantum error correction (QEC) codes suppress errors by encoding logical quantum information in many redundant physical qubits [4–7]. An important class of QEC codes are Calderbank-Shor-Steane (CSS) codes [8, 9], which includes surface codes [10], color codes [11] and bicycle quantum low-density parity check (QLDPC) codes [12–14]. Such CSS codes have been realized experimentally on various platforms [15–17].

In QEC, the key idea is to perform measurements on the physical system affected by errors, while not destroying the encoded logical information. From such syndrome measurements, one can infer whether an error has occurred, and which operation is best suited to correct the error to recover the original logical information. Here, a key challenge in QEC is decoding, i.e. inferring which is the most likely error that has occurred given the syndrome measurements. Decoding is a challenging computational problem [18] which has to be solved accurately in as short time as possible. Various types of decoders have been proposed over the years, where decoders usually have to balance a tradeoff between high speed and high correction accuracy. This includes decoders based on tensor-networks [19–21], neural networks [22], annealing [23–25], belief-propagation [26, 27], perfect weight-matching [28–30], renormalization group [31], and union-find [32].

A recent approach proposed to decode via mapping to the maximum satisfiability (MaxSAT) problem [33], which has been shown to provide a highly accurate decoder. However, so far the MaxSAT decoder has been limited to color codes and uniform noise models.

Here, we decode arbitrary CSS codes with high accuracy by mapping them into MaxSAT problems. Our decoder corresponds to the quantum maximum likelihood decoder [18] with a completely general construction that works for any CSS code, including biased non-uniform noise models and noisy syndrome measurements. We find that our decoder has the similar computational scaling as belief-propagation with ordered statistic post-processing (BP-OSD), while achieving superior decoding accuracy. In particular, for the color code our MaxSAT decoder has a higher threshold and better scaling of noise suppression with distance compared to BP-OSD, while showing similar scaling in computational time. We also demonstrate higher accuracy for the recently proposed bicycle QLDPC codes by IBM [13] and surface codes. We relate the complexity of the MaxSAT decoding problem to a computational phase transition, showing that our mapping is in the easy computational phase. Our decoder can be directly implemented on ASICs and FPGAs, which promises to dramatically speed up decoding and opens up the possibility of real-time decoding. Our approach provides a powerful and flexible framework to enhance QEC.

First, in Sec. II we introduce QEC, decoding and MaxSAT. Then, in Sec. III we show how to map the quantum decoding problem of general CSS codes into a MaxSAT problem and extend our construction to include noisy measurements. In Sec. IV, we show the relationship between the decoding problem and the complexity phase transition of MaxSAT. We introduce our methods in Sec. V and numerical decoding results in Sec. VI. Finally, we discuss our results and conclude in Sec. VII.

* Corresponding author: mrn31@cam.ac.uk

† tobias.haug@u.nus.edu

II. PRELIMINARIES

We start by introducing the basics of QEC and MaxSAT.

A. Quantum Maximum likelihood decoding

A quantum error-correcting code $[[n, k, d]]$ has n data qubits, k logical qubits and code distance d . For a CSS code, the full parity check matrix

$$H = \begin{pmatrix} 0 & H_X \\ H_Z & 0 \end{pmatrix} \quad (1)$$

is composed of parity check matrix H_Z with only Z Pauli parity checks, and H_X with only X checks. These stabilizer generators commute, which is ensured by the condition $H_X \cdot H_Z^T = 0$. H_X reveals phase (Z) errors, while H_Z is responsible to detect bit-flip (X) errors. The parity checks act on n data qubits, where we assume that the j th data qubit is subject to X Pauli errors with probability p_j^X , Z Pauli errors with probability p_j^Z and Y Pauli errors with probability p_j^Y .

We decode H_X and H_Z separately, where we now illustrate the decoding for the $m \times n$ matrix H_Z (H_X follows analogously)

$$H_Z = \begin{pmatrix} h_{11} & h_{12} & \cdots & h_{1n} \\ h_{21} & h_{22} & \cdots & h_{2n} \\ \vdots & \vdots & \ddots & \vdots \\ h_{m1} & h_{m2} & \cdots & h_{mn} \end{pmatrix}$$

where each element h_{ij} is either 1 or 0, indicating whether qubit j participates in parity check i or not, and m is the number of parity checks (rows), each having a Hamming weight $\omega_i = \sum_j h_{ij}$. Physically, the i th parity check corresponds to measuring the Pauli string $\sigma_i = \otimes_{j=1}^n Z^{h_{ij}}$. Measuring the m parity checks yields a syndrome outcome $\mathbf{s} = (s_1, s_2, \dots, s_m)$ with $s_i \in \{0, 1\}$. Given the syndrome, the parity check constraint $\mathbf{s} = H_Z \mathbf{e}$, fixes the error configuration $\mathbf{e} = \{e_1, \dots, e_n\}$ with $e_j \in \{0, 1\}$ indicating whether a bit-flip error has occurred for qubit j . Given the measured syndrome \mathbf{s} , one wants now to figure out which is the actual error that has occurred. The quantum maximum likelihood decoding problem finds the error configuration with the highest probability given the constraints of the syndrome [18].

The probability that a bit-flip error configuration \mathbf{e} has occurred is given by [30]

$$P(\mathbf{e}) = \prod_{j=1}^n (1 - p_j)^{1 - e_j} p_j^{e_j} = \left[\prod_{j=1}^n (1 - p_j) \right] \prod_{j=1}^n \left(\frac{p_j}{1 - p_j} \right)^{e_j}, \quad (2)$$

where $p_j = p_j^X + p_j^Y$ is the probability that an X or Y error has affected the j th qubit, which both induce a bit-flip. To find the most probable error \mathbf{e}^{ml} given the measured syndrome \mathbf{s} , one has to maximize the log-likelihood

$$\mathbf{e}^{\text{ml}} = \arg \max_{\mathbf{e}} \{\ln(P(\mathbf{e}))\} = \arg \max_{\mathbf{e}} \left(C - \sum_j w_j e_j \right) \quad (3)$$

$$\text{s.t. } \mathbf{s} = H_Z \mathbf{e}, \quad (4)$$

where we have the irrelevant constant $C = \sum_j \ln(1 - p_j)$ and weights $w_j = \ln((1 - p_j)/p_j)$ which represent the log-likelihood ratio between the probabilities of no error and a bit-flip error on the j th qubit based on the prior p_j .

B. MaxSAT

MaxSAT is an optimization variant of the Boolean satisfiability (SAT) problem where one aims to find an assignment of binary variables such that it satisfies maximum number of clauses. The MaxSAT instance is constructed in a standard and widely used format called conjunctive normal form (CNF). For a summary of terms and conventions see Appendix A. A k -SAT instance, is a specific case of a Boolean satisfiability problem in which one is given a Boolean expression written in CNF form where each clause is constrained to k literals. As an example, below we have a CNF formula for two boolean variables e_1 and e_2 (also called literals) consisting of three 2-SAT clauses

$$(e_1 \vee e_2) \wedge (e_1 \vee \neg e_2) \wedge (\neg e_1 \vee e_2), \quad (5)$$

where \neg is the negation of the literal, \vee indicates a logical OR and \wedge a logical AND. In above example, the choice $e_1 = e_2 = 1$ satisfies all three clauses, thus being the solution of the SAT problem.

III. MAXSAT FORMULATION OF THE DECODING PROBLEM

We now map the decoding problem of arbitrary CSS code into a MaxSAT problem.

A. CNF Construction

As first step, we deal with the constraints due to the given syndrome (4), which turns out to be a SAT problem. We expand (4) to get m binary addition (XOR) equations

$$s_i = h_{i1}e_1 \oplus h_{i2}e_2 \oplus \cdots \oplus h_{in}e_n. \quad (6)$$

As variables e_j with $h_{ij} = 0$ do not contribute, each constraint s_i involves only $\omega_i = \sum_j h_{ij}$ variables. The strategy to transform the above constraints to CNF clauses starts with giving a Boolean variable interpretation to the binary elements e_j , agreeing that True evaluates to binary value 1. In order to be able to construct k -SAT clauses, we need to break down the RHS of the (6) to expressions involving less number of literals. In particular, we break down the i th constraint in (6) to smaller expressions by introducing a set of auxiliary literals $\{a_1, a_2, \dots, a_{n-1}\}$ to save the result of the intermediate expres-

sions in

$$\begin{cases} a_1 = h_{i1}e_1 \oplus h_{i2}e_2 \\ a_2 = a_1 \oplus h_{i3}e_3 \\ a_3 = a_2 \oplus h_{i4}e_4 \\ \vdots \\ a_{n-3} = a_{n-4} \oplus h_{i(n-2)}e_{n-2} \\ s_i = a_{n-2} \oplus h_{in}e_n \end{cases} \quad (7)$$

As mentioned before, the weight of each parity check is $\omega_i = \sum_j h_{ij}$, which means that out of n elements $h_{i1}, h_{i2}, \dots, h_{in}$ only ω_i of them are non-zero and need to be taken into account for evaluation of the i^{th} constraint. The number of equations in (7) also would reduce to $\omega_i - 2$. Note that h_{ij} and s_i are known binary values in the above set of equations. There are various types of equations above that have a different form of translation to 3-SAT clauses. Tab. I summarises the prescription for each type of equation to be translated to a 3-SAT CNF. We will later explain the motivation behind choosing clauses with length 3.

For the proposed mapping, we have $\omega_i - 2$ number of constraints in (7) and each of them would translate to 4 clauses as described in Tab. I. Thus, the total number of clauses is $4 \sum_i (\omega_i - 2)$.

B. Soft Clauses

Next, we deal with finding the most likely error under the syndrome constraints, which is described by the maximisation condition (3).

MaxSAT algorithms allow for introducing a weight associated with each soft clause, which would be the cost of violating that particular clause. In this context, hard clauses are considered as infinite-weight clauses, which means that even if one of the hard clauses is violated, the solver has failed to find a satisfying assignment.

In the language of MaxSAT, the log-likelihood maximisation in (3) can be described as a set of weighted soft clauses. One can drop the negative sign in front of the log-likelihood in (3) and then the weights w_i can be interpreted as costs of soft clauses to be minimised. Here, it is worth noting that the most likely error configuration is not necessarily the one with least Hamming weight, which was the assumption in [33], although this is a valid assumption for uniform error probabilities. Therefore, for probabilities $p_j < 0.5$, the corresponding MaxSAT soft clause is the negation of the error literal e_i with corresponding weight w_j as its cost, as shown in Tab. I, while for $p_j \geq 0.5$ a slight modification is necessary.

To turn the soft clauses into 3-SAT clauses, we require $2n$ auxiliary literals $\{b_1, \dots, b_{2n}\}$ and the total number of soft clauses would be $4n$; see Tab. I.

We stress that in our MaxSAT formulation, the error probabilities p_j for each data qubit j can be chosen arbitrarily. Further, our mapping applies to parity check matrix of arbitrary CSS codes. We note that the MaxSAT decoder of Ref. [33] only supports uniform p_j , and is restricted to the color code.

C. Measurement error

So far, we considered the decoding problem where we assume that syndrome measurements are not affected by noise. We now handle noisy syndrome measurements via a phenomenological error model [28]. Here, we assume that the syndrome outcome of the i^{th} parity check measurement is flipped with probability q_i . Now, a non-zero syndrome outcome may indicate that either an error occurred on the data qubits or on the measurement itself. To be able to pinpoint the origin of the error, one repeats the syndrome measurement L times (with usually $L = d$), and pinpoints the error by performing parity checks across both the data qubits and consecutive noisy syndromes. As before, we can decode X and Z errors separately, where we now illustrate decoding H_Z for X errors.

We denote the index of measurement repetition by $t = 1, \dots, L$. Errors on the data qubits that happen during the t^{th} iteration are given by $\mathbf{e}^t = \{e_1^t, \dots, e_n^t\}$ where each error happens with probability p_j . Additionally, errors in the syndrome measurement during the t^{th} measurement is described by the binary list $\mathbf{r}^t = \{r_1^t, \dots, r_m^t\}$. The quantum maximum likelihood decoding problem can be written as

$$\begin{aligned} (\mathbf{e}^{\text{ml}}, \mathbf{r}^{\text{ml}}) &= \arg \max_{\mathbf{e}, \mathbf{r}} \{\ln(P(\mathbf{e}, \mathbf{r}))\} \\ &= \arg \max_{\mathbf{e}, \mathbf{r}} \left(C' - \sum_{j=1}^n \sum_{t=1}^L w_j e_j^t - \sum_{i=1}^m \sum_{t=1}^{L-1} u_i r_i^t \right) \quad (8) \\ \text{s.t. } \mathbf{s}' &= H_Z' \mathbf{y}, \quad (9) \end{aligned}$$

where $u_i = \ln((1 - q_i)/q_i)$ are the weights for the syndrome error probability, $\mathbf{s}' = \{s^1, s^1 \oplus s^2, \dots, s^{L-1} \oplus s^L\}$ the difference between consecutive syndrome outcomes with noisy syndrome $\mathbf{s}^t \in \{0, 1\}^m$ measured at the t^{th} repetition, error configuration vector $\mathbf{v} = \{\mathbf{e}^1, \mathbf{r}^1, \mathbf{e}^2, \mathbf{r}^2, \dots, \mathbf{e}^{L-1}, \mathbf{r}^{L-1}, \mathbf{e}^L\}$ combining data and measurement error literals, and the parity check matrix including measurement errors H_Z' (which is a $mL \times (nL + m(L - 1))$ matrix) given by

$$H_Z' = \begin{pmatrix} H_Z & I_m & 0 & 0 & 0 & 0 & \dots & 0 & 0 & 0 & 0 \\ 0 & I_m & H_Z & I_m & 0 & 0 & \dots & 0 & 0 & 0 & 0 \\ 0 & 0 & 0 & I_m & H_Z & I_m & \dots & 0 & 0 & 0 & 0 \\ 0 & 0 & 0 & 0 & 0 & I_m & \dots & 0 & 0 & 0 & 0 \\ \vdots & \vdots & \vdots & \vdots & \vdots & \vdots & \ddots & \vdots & \vdots & \vdots & \vdots \\ 0 & 0 & 0 & 0 & 0 & 0 & \dots & I_m & 0 & 0 & 0 \\ 0 & 0 & 0 & 0 & 0 & 0 & \dots & I_m & H_Z & I_m & 0 \\ 0 & 0 & 0 & 0 & 0 & 0 & \dots & 0 & 0 & I_m & H_Z \end{pmatrix}$$

with I_m being the $m \times m$ identity matrix. Note that one can assume that the measurement of the last syndrome is noise-free. Now, each parity checks of H_Z' (i.e. each row) has $\omega_i + 2$ non-zero terms (except in the first and last repetition), where ω_i terms interact with data qubit errors and 2 terms with measurement errors. Checks related to the first and last repetition have only $\omega_i + 1$ terms: This is because the first check has no preceding error syndrome, while for the last repetition we assume that the last syndrome measurement is noise-free. Note

Type of Equation	Example	Translation to 3-SAT CNF
$n \geq 2$:		
1. Equations involving 3 literals	$a_1 = e_1 \oplus e_2$	$(\neg e_1 \vee \neg e_2 \vee \neg a_1) \wedge$ $(e_1 \vee e_2 \vee \neg a_1) \wedge$ $(\neg e_1 \vee e_2 \vee a_1) \wedge$ $(e_1 \vee \neg e_2 \vee a_1)$
2. Last equation with $s_i = 0$ Note: In this case we need the last auxiliary variable a_{n-1} to achieve the 3-SAT clause form	$0 = a_{n-2} \oplus e_n$	$(\neg a_{n-2} \vee e_n \vee a_{n-1}) \wedge$ $(\neg a_{n-2} \vee e_n \vee \neg a_{n-1}) \wedge$ $(a_{n-2} \vee \neg e_n \vee a_{n-1}) \wedge$ $(a_{n-2} \vee \neg e_n \vee \neg a_{n-1})$ <i>Note: Logic equivalent to $(a_{n-2} = e_n)$</i>
3. Last equation with $s_i = 1$ Note: In this case we need the last auxiliary variable a_{n-1} to achieve the 3-SAT clause form	$1 = a_{n-2} \oplus e_n$	$(a_{n-2} \vee e_n \vee a_{n-1}) \wedge$ $(a_{n-2} \vee e_n \vee \neg a_{n-1}) \wedge$ $(\neg a_{n-2} \vee \neg e_n \vee a_{n-1}) \wedge$ $(\neg a_{n-2} \vee \neg e_n \vee \neg a_{n-1})$ <i>Note: Logic equivalent to $(a_{n-2} \neq e_n)$</i>
Weighted Soft Clauses	Example	Translation to 3-SAT CNF
1. If $w_j < 0$: literal Note: To achieve a 3-SAT form we need 2 auxiliary variables. Let's call them b_{2j} and b_{2j+1}	$ w_j e_j$	$ w_j (e_j \vee b_{2j} \vee b_{2j+1}) \wedge$ $ w_j (e_j \vee \neg b_{2j} \vee b_{2j+1}) \wedge$ $ w_j (e_j \vee b_{2j} \vee \neg b_{2j+1}) \wedge$ $ w_j (e_j \vee \neg b_{2j} \vee \neg b_{2j+1})$
2. If $w_j \geq 0$: negated literal Note: To achieve a 3-SAT form we need 2 auxiliary variables. Let's call them b_{2j} and b_{2j+1}	$w_j \neg e_j$	$w_j (\neg e_j \vee b_{2j} \vee b_{2j+1}) \wedge$ $w_j (\neg e_j \vee \neg b_{2j} \vee b_{2j+1}) \wedge$ $w_j (\neg e_j \vee b_{2j} \vee \neg b_{2j+1}) \wedge$ $w_j (\neg e_j \vee \neg b_{2j} \vee \neg b_{2j+1})$

TABLE I. Prescriptions for translating different types of equations or soft clauses to 3-SAT (weighted) CNF form.

that for the case $L = 1$, we recover the noiseless syndrome decoding problem in (3) and (4).

Similar to the noise-free syndrome measurement case, the decoding problem including measurement noise can be mapped into a MaxSAT instance. The key point to note is that all L rounds of the syndrome measurements for every m parity checks of H_Z are decoded simultaneously as implied by the extended parity check matrix H'_Z in (9). The corresponding hard constraint equations for all mL parity checks (indexed below by i) is given consistently by (similar to (6))

$$s'_i = h'_{i,1} v_1 \oplus h'_{i,2} v_2 \oplus \dots \oplus h'_{i,(nL+m(L-1))} v_{(nL+m(L-1))}. \quad (10)$$

where we used the previously introduced vector of error variables \mathbf{v} , syndrome differences s' and matrix elements h'_{ij} of H'_Z . The breakdown of equations in (10) into smaller ones for mapping to 3-SAT clauses is analogue to (7), which we avoid repeating here for brevity. The Tab. I contains all the necessary and sufficient rules to obtain the 3-SAT form of the *XOR* equations for this case.

The soft clauses is constructed similarly as before with now two weight vectors, namely w_j for the qubit literals and u_i for syndrome literals.

IV. CLAUSE DENSITY AND COMPLEXITY

A key factor in complexity of solving MaxSAT instances is the clause density α . In the study of computational complex-

ity, the clause density of a random k -SAT problem is defined as the ratio of the number of clauses μ to the number of literals ν , denoted by $\alpha = \mu/\nu$. The hardness phase transition for k -SAT problems is a critical concept, highlighting a threshold clause density α_c at which the problems transition from being predominantly solvable to predominantly unsolvable. If we represent the class of random k -SAT problems with ν literals and μ clauses as $\mathcal{R}_k(\nu, \mu = \alpha\nu)$, then the hardness phase transition can be written as the discontinuity in the success probability of finding a satisfying assignment to the problems as a function of clause density (the order parameter) [34]

$$\lim_{\nu \rightarrow \infty} \text{Prob}(\text{sat}, \mathcal{R}_k(\nu, \alpha\nu)) = \begin{cases} 0, & \text{if } \alpha > \alpha_c \\ 1, & \text{if } \alpha < \alpha_c \end{cases} \quad (11)$$

For different values of k , the critical clause density where this phase transition occurs varies. For $k = 2$, the phase transition occurs at $\alpha_c \approx 1.0$ [34]. For $k = 3$, the phase transition occurs at $\alpha_c \approx 4.2$ [34], a widely studied and critical threshold in the theory of NP-completeness. For $k = 4$, the phase transition is observed at $\alpha \approx 9.8$ [34]. The direct relevance of these transitions in the context of QEC decoding, is in the scaling of the time to solution. For example, it has been shown that for random 3-SAT instances at $\alpha_c > 5.6$, resolution algorithms need *exponential time* to get a probability of success near 1 [34, 35]. Therefore, the study of the complexity phase transition provides a theoretical framework for expecting a sudden shift in the solvability of the problems as the clause density crosses these thresholds. For a detailed dis-

cussion see also Ref. [36]. Therefore, the critical clause density can have important implications on whether it is feasible to use SAT solvers as QEC decoders and which QEC codes would be ideal for these solvers.

Apart from the hardness phase transition as a factor to consider in choosing the clause length, it is also important to note that lower clause lengths are more desirable. This is due to the fact that designing a hardware SAT solver for lower k values is easier. In other words, one can think of a clause as a k -body interaction term where we opt to use 3-body terms.

Optimally we would like the CNF of the decoding problem to be in the easy phase $\alpha < \alpha_c$.

Now we bound the clause density for generic CSS codes (assuming no syndrome measurement errors). Assuming the n -qubit code has m parity checks each with Hamming weight ω_i , then for the 3-SAT construction in Tab. I the clause density is given by

$$\alpha^{3\text{-SAT}} = \frac{\# \text{ clauses}}{\# \text{ literals}} = \frac{\sum_{i=1}^m 4(\omega_i - 2)}{n + \sum_{i=1}^m (\omega_i - 1)} \quad (12)$$

For common CSS codes such as the Toric code, one has $m \approx n/2$. To get a simple formula for α , let us consider $m \leq n$. Therefore, we get $\alpha \leq 4 - \frac{8}{\omega} \leq 4$. In particular, the clause density always remains below the phase transition $\alpha_c \approx 4.2$, which holds in fact for any m .

Similarly, one can also consider the clause density for the MaxSAT decoding including the soft clauses that encode the error probability. For a homogeneous Max-3-SAT CNF formula, the clause density is

$$\alpha^{\text{Max-3-SAT}} = \frac{\# \text{ clauses}}{\# \text{ literals}} = \frac{4n + \sum_{i=1}^m 4(\omega_i - 2)}{3n + \sum_{i=1}^m (\omega_i - 1)} \quad (13)$$

Addition of soft clauses in fact reduces the clause density, giving us again an upper bound of $\alpha \leq 4$ for any m . It was shown that critical value of the clause density at the phase transition point for random Max- k -SAT instances is similar to the random k -SAT ones [37].

As an example, we now estimate $\alpha^{3\text{-SAT}}$ for the triangular 6.6.6 color code used in (4). This code is on a lattice with triangular geometry and hexagonal lattice tiles, where tiles are also referred to as faces or parity checks. In such a lattice, the distance of the code d is the linear dimension of the lattice (length of one side), and the total number of qubits present is proportional to $\frac{3d^2+1}{4}$. The total number of faces (parity checks) is also proportional to $\frac{3d^2+1}{8}$. As explained in previous sections, we need $4(\omega_i - 2)$ 3-SAT clauses for i^{th} parity check. For the considered color code, $\omega_i \in \{4, 6\}$. Since the majority of the parity checks have weight 6, we pick $\omega_i = \omega = 6$ to estimate an upper-bound for the clause density. Therefore the total number of clauses is proportional to $4(\omega - 2)\frac{3d^2+1}{8} \propto 6d^2$. Now we need to estimate the number of literals used in each instance. It is straightforward to show that the number of literals is proportional to $\frac{3d^2+1}{4} + \frac{3d^2+1}{8}(\omega - 1) \propto 2.6d^2$. Therefore, the clause density is $\alpha^{3\text{-SAT}} = \frac{6d^2}{2.6d^2} \approx 2.3$ which is significantly less than $\alpha_c = 4.2$. Thus, with the proposed construction the color code is deeply within the *easy* phase of MaxSAT even when scaling up the code size.

The clause density calculation for the case including noisy syndrome measurements follows similar to (12) and (13). The main differences are the number of parity checks which have increased by L times for H'_Z and each of them now involve $4\omega_i$ 3-SAT clauses (except for $i \in \{1, mL\}$ where there are $4(\omega_i - 1)$ clauses) and additionally the number of error variables has increased to nL qubit error variables represented by \mathbf{e} and $m(L - 1)$ syndrome error variables represented by \mathbf{r} (see (8)). Finally, for soft clauses, we need to add the contribution of the qubit and syndrome error variables. For qubit error variables we get a total of $4nL$ soft clauses and $2nL$ auxiliary variables whereas for syndrome error variables we get $4m(L - 1)$ additional soft clauses and $2m(L - 1)$ additional auxiliary literals. Therefore the clause density for the hard constraints is

$$\alpha^{3\text{-SAT}} = \frac{\sum_{i=1}^{mL} 4\omega_i}{nL + m(L - 1) + \sum_{i=1}^{mL} (\omega_i + 1)} \quad (14)$$

and for MaxSAT with both soft and hard constraints is given by

$$\alpha^{\text{Max-3-SAT}} = \frac{4nL + 4m(L - 1) + \sum_{i=1}^{mL} 4\omega_i}{3nL + 3m(L - 1) + \sum_{i=1}^{mL} (\omega_i + 1)} \quad (15)$$

As an example, for the 6.6.6 color code, we get $\alpha^{\text{Max-3-SAT}} \approx 2.5$. We note that again $\alpha^{\text{Max-3-SAT}} \leq 4$, i.e. the MaxSAT problem always remains in the *easy* computational phase.

V. METHODS

To solve MaxSAT, we assessed the performance of various MaxSAT solvers and the best performing algorithm was chosen to carry out the experiments. Based on qualitative and quantitative results, among various solvers such as CASHWMaxSAT-CorePlus, CGSS2, EvalMaxSAT, OpenWBO, Pacose and Loandra [38], Open-WBO proved to be the best solver.

To evaluate the performance of our MaxSAT decoder, we compare against another popular decoder that runs on arbitrary CSS codes, namely belief propagation with the ordered statistics postprocessing step decoder (BP-OSD) which was proposed in Ref. [26, 27]. BP-OSD relies on belief propagation, a heuristic message passing algorithm that estimates the single-bit marginals of a probability distribution, with an ordered statistics postprocessing step to determine the most likely error. BP-OSD has been shown to work well for bivariate bicycle QLDPC codes [12] such as the codes proposed in Ref. [13].

For both MaxSAT and BP-OSD, we decode H_X and H_Z separately, giving us the total decoded qubit error $\mathbf{e}_{\text{dec}} = \bigoplus_{t=1}^L \mathbf{e}^t$. We compute the remaining error after correction $\delta\mathbf{e} = \mathbf{e}^* \oplus \mathbf{e}_{\text{dec}}$ by adding the decoded data qubit error onto the actual error configuration \mathbf{e}^* . The logical error rate p_L is given by the probability that after correction the remaining error $\delta\mathbf{e}$ anti-commutes with at least one of the logical operators of the k logical qubits.

As error model, we assume single-qubit depolarizing noise

$$\mathcal{E}_p(\rho) = (1 - p)\rho + p/3(X\rho X + Y\rho Y + Z\rho Z) \quad (16)$$

with physical error rate $p_j^X = p_j^Z = p_j^Y = p/3$ which are uniform for every qubit j . Further, we assume noise-free syndrome measurements $q_j = 0$ and one repetition $L = 1$, i.e. we study the code capacity.

To characterize the error capabilities of our codes, we study the scaling of the logical error p_L against physical error rate p with the heuristic formula [13, 39]

$$p_L(p) = p^{d_{\text{fit}}/2} \exp(c_0 + c_1 p + c_2 p^2). \quad (17)$$

For surface codes and bicycle codes [13, 14] it has been observed that the fitted distance corresponds to the actual distance via $d_{\text{fit}}/2 = \lceil d/2 \rceil$ [39].

We also study the pseudo threshold $p_{\text{p-th}}$. It is defined as the error probability satisfying the break-even relation [13]

$$p_L(p_{\text{p-th}}) = 1 - (1 - p_{\text{p-th}})^k \quad (18)$$

where the probability of a logical error is equivalent to the probability of at least one unencoded physical qubit suffering an error.

VI. RESULTS

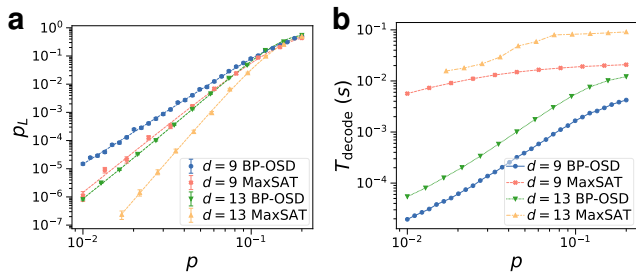


FIG. 1. Performance of our MaxSAT decoder and BP-OSD decoder against physical error rate p for the Color code. **a)** Logical error rate p_L against p . Dashed line is fit with (17) with $d_{\text{fit}}^{\text{BP-OSD}} = 7.3$ and $d_{\text{fit}}^{\text{MaxSAT}} = 9.6$ for $d = 9$, and $d_{\text{fit}}^{\text{BP-OSD}} = 9.2$ and $d_{\text{fit}}^{\text{MaxSAT}} = 13.8$ for $d = 13$. We find pseudo-thresholds $p_{\text{p-th}}^{\text{BP-OSD}} = 0.109$ and $p_{\text{p-th}}^{\text{MaxSAT}} = 0.122$ for $d = 9$, while $p_{\text{p-th}}^{\text{BP-OSD}} = 0.112$ and $p_{\text{p-th}}^{\text{MaxSAT}} = 0.130$ for $d = 13$. **b)** Decoding time T_{decode} against p .

First, we study the 6.6/6 or Honeycomb Color code [11] for our MaxSAT decoder and BP-OSD against distance d of the code. Its code parameters are given by $[[(3d^2 + 1)/4, 1, d]]$. We show the logical error rate p_L against physical error rate p in Fig. 1a. We study the MaxSAT decoder and BP-OSD for different distances d . We find that MaxSAT decoder has superior scaling in error suppression. In particular, from the fit with (17), we find the optimal scaling $d_{\text{fit}} \approx d$ for the MaxSAT decoder. In contrast, for BP-OSD we only find a reduced $d_{\text{fit}} \approx 3/4d$, indicating that the BP-OSD decoder can miss errors even with weight smaller than $d/2$.

Next, we study p_L against distance d for fixed error $p = 0.1$ in Fig. 2a. We find that our MaxSAT decoder has vastly lower logical error rate compared to BP-OSD. Both codes decrease the error exponentially $p_L \propto \exp(-\gamma d)$ with distance d . However, MaxSAT decoding shows a twice as fast decay $\gamma_{\text{MaxSAT}} \approx 0.14$ with d compared to BP-OSD with $\gamma \approx 0.06$. Thus, our MaxSAT decoder achieves the same noise suppression as BP-OSD at only half the code distance. Thus, our decoder yields a reduction of a factor 4 in terms of physical qubit number compared to BP-OSD. We note that the reduced performance of BP-OSD for color codes has also been noted in Ref. [40].

We show the time T_{decode} needed to decode against number of data qubits n in Fig. 2b. We find that MaxSAT decoder and BP-OSD decoder show similar scaling $T_{\text{decode}} \propto n^\beta$, with $\beta \approx 3/2$. We note that our MaxSAT decoder runs about an order of magnitude slower than BP-OSD. We note that our current implementation runs only on CPU, and an optimised implementation on specialized hardware can speed up the MaxSAT decoder substantially [41].

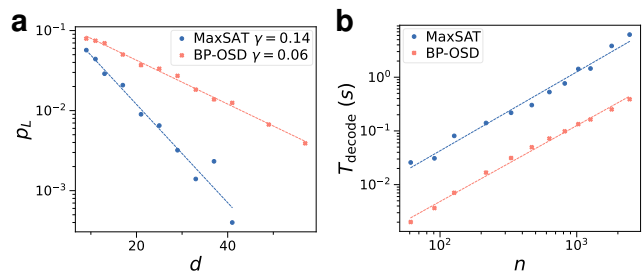


FIG. 2. Scaling of MaxSAT and BP-OSD decoder for the Color code with error probability $p = 0.1$. **a)** Logical error rate p_L against distance d . Dashed line is fit with $p_L \propto \exp(-\gamma d)$ where we find $\gamma_{\text{MaxSAT}} \approx 0.14$ and $\gamma_{\text{BP-OSD}} \approx 0.06$. **b)** Decoding time T_{decode} against number of data qubits n . Dashed line is fit with $T_{\text{decode}} \propto n^\beta$ with $\beta_{\text{MaxSAT}} \approx 1.46$ and $\beta_{\text{BP-OSD}} \approx 1.41$.

Next, in Fig. 3 we study the decoding of the QLPDC codes recently introduced by IBM [13]. In Fig. 3a, we show a $[[108, 8, 10]]$ code, where we find that our MaxSAT decoder shows about three times lower logical error rates compared to the BP-OSD decoder [26], which was also used in Ref. [13]. In Fig. 3b, we study the $[[144, 12, 12]]$ QLPDC code, where we find that our MaxSAT decoder has lower logical error rates compared to BP-OSD. We note that the logical error rate shows comparable scaling with p for both MaxSAT and BP-OSD evident by similar values for d_{fit} .

We study the threshold of the Color code in Fig. 4 under depolarizing noise. We find that curves for different d all intersect at the same physical error, which is the threshold p_{th} . We apply the critical scaling ansatz $p_L = f(d^\nu(p - p_{\text{th}}))$, with f being a degree-2 polynomial, to fit p_{th} and exponent ν [42]. When appropriately rescaled, curves for all d collapse onto a single curve around the threshold. We find that the MaxSAT decoder has a higher fitted threshold of $p_{\text{th}} = 15.20$ compared to the BP-OSD with $p_{\text{th}} = 13.23$.

Finally, we study the logical error rate p_L against physical error p for the rotated surface code [43] in Fig. 5. We find

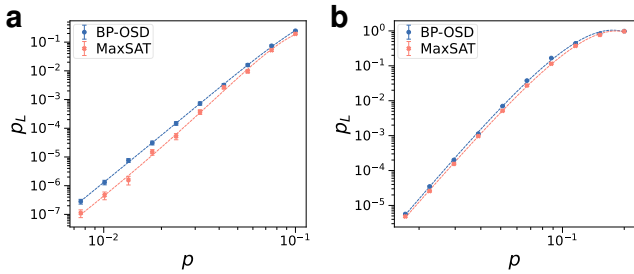


FIG. 3. Performance for decoding the QLDPC codes introduced by IBM [13] MaxSAT decoders and BP-OSD decoder. We show logical error rate p_L against physical error rate p . Dashed line is fit with (17). **a)** $[[108, 8, 10]]$ QLDPC code with $d_{\text{fit}}^{\text{BP-OSD}} = 10.7$, $d_{\text{fit}}^{\text{BP-OSD}} = 9.8$. **b)** $[[144, 12, 12]]$ QLDPC code with $d_{\text{fit}}^{\text{BP-OSD}} = 14.2$, $d_{\text{fit}}^{\text{BP-OSD}} = 13.7$.

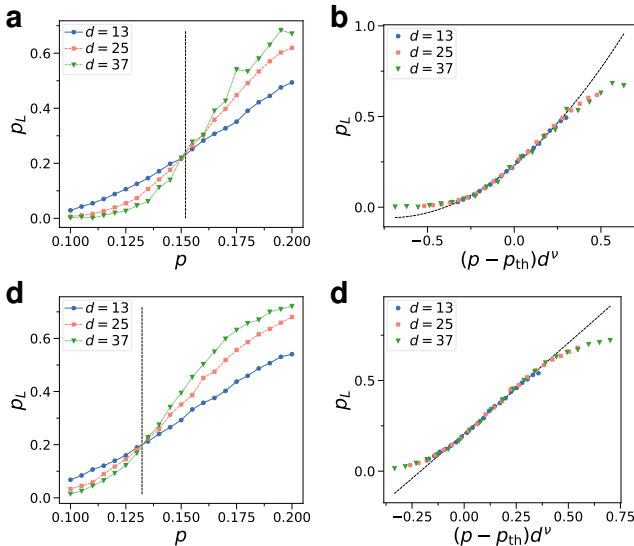


FIG. 4. Threshold of Color code for **a,b)** MaxSAT and **c,d)** BP-OSD decoder for depolarizing noise. **a,c)** We show logical error p_L against physical error p for different distances d with fitted threshold $p_{\text{th}} = 15.20 \pm 0.05\%$ for MaxSAT and $p_{\text{th}} = 13.23 \pm 0.04\%$ for BP-OSD, indicated as dashed vertical line. **b,d)** Rescaled error around threshold p_{th} of fit with exponent $\nu = 0.71$ for MaxSAT and $\nu = 0.65$ for BP-OSD, where dashed line is the fitted critical scaling ansatz.

that the MaxSAT decoder has slightly lower logical error rates compared to the BP-OSD decoder.

VII. DISCUSSION

We demonstrate MaxSAT to decode arbitrary CSS codes with high accuracy. We show how to map the quantum maximum likelihood decoding problem of CSS codes into Max-3-SAT instances. Our mapping supports CSS codes with parity checks of any weight and geometry, and can handle biased single-qubit Pauli noise with non-uniform error probabilities across different data qubits. Further, our decoder handles noisy syndrome measurements within the commonly used phenomenological error model.

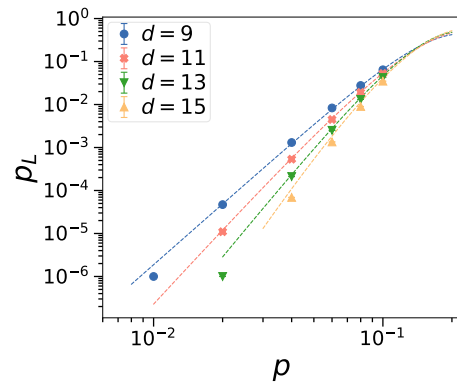


FIG. 5. Logical error rate p_L against physical error rate p for the rotated surface code for different distances d . Dots are MaxSAT solver results, while dashed line is BP-OSD.

The computational complexity of solving MaxSAT is related to a computational phase transition at a critical clause density of the MaxSAT problem. We show that the clause density of our mapping is always below the critical clause density, thus remaining in the *easy* phase of MaxSAT. Thus, we expect our decoder to perform well even when scaling up the code size.

Code	MaxSAT	BP-OSD
Toric Code (2D)	15.55 ± 0.03	14.86 ± 0.03
Color Code (on hexagonal lattice)	15.20 ± 0.05	13.23 ± 0.04

TABLE II. Comparison of Error Thresholds (%) for MaxSAT and BP-OSD decoders under uniform depolarizing noise.

We demonstrate that MaxSAT can decode the Color code effectively, showing a superior code capacity threshold compared to BP-OSD as summarized in Tab. II. Further, we find that MaxSAT decoding gives the asymptotically optimal scaling of $p_L \sim p^{d/2}$, while BP-OSD only reaches a sub-optimal scaling of $p_L \sim p^{\eta d/2}$ with $\eta \approx 3/4$. From a scaling analysis in Fig. 2, our decoder allows a factor 4 reduction in number of data qubits while offering similar noise protection than BP-OSD.

We also study recently proposed QLDPC codes [13], finding improved accuracy compared to BP-OSD. Our solver also has a higher threshold for the Toric code compared to BP-OSD, and slightly lower error rates for the rotated surface code.

We highlight that our MaxSAT decoder can be directly applied to arbitrary CSS codes as a quantum maximum likelihood decoder to find the most probable error. This contrasts more specialized decoders such as minimum-weight perfect matching (MWPM), which require that each error affects at most two decoders, i.e. each column of H has at most two non-zero entries [28, 29, 44], and extensions to other codes require purpose-built modifications [45–47] or relaxations [48].

We find improved performance across different types QEC codes, and thus expect MaxSAT decoding to be robust to the specific implementation and application. In current

work, while the decoder shows promising scaling with n , the solvers are still relatively slow in absolute computational time. However, we stress that we ran the MaxSAT solver serially on CPU, which leaves a lot of room for improvement in terms of speed-up. In particular, the solvers can

be parallelised [49] and implemented on specialized hardware [41] such as Field Programmable Gate Arrays (FPGAs) and Application-specific integrated circuits (ASICs), which can result in speed-ups of several orders of magnitude. Thus, our approach promises application as practical and highly accurate decoders to enable quantum computing.

-
- [1] P. W. Shor, Polynomial-time algorithms for prime factorization and discrete logarithms on a quantum computer, *SIAM review* **41**, 303 (1999).
- [2] M. A. Nielsen and I. L. Chuang, *Quantum computation and quantum information*, Vol. 2 (Cambridge university press Cambridge, 2001).
- [3] M. Noormandipour and H. Wang, Matching point sets with quantum circuit learning, in *ICASSP 2022 - 2022 IEEE International Conference on Acoustics, Speech and Signal Processing (ICASSP)* (2022) pp. 8607–8611.
- [4] P. W. Shor, Fault-tolerant quantum computation, in *Proceedings of 37th conference on foundations of computer science* (IEEE, 1996) pp. 56–65.
- [5] D. J. MacKay and R. M. Neal, Near Shannon limit performance of low density parity check codes, *Electronics letters* **33**, 457 (1997).
- [6] S. Resch and U. R. Karpuzcu, Benchmarking quantum computers and the impact of quantum noise, *ACM Computing Surveys (CSUR)* **54**, 1 (2021).
- [7] S. M. Girvin, Introduction to quantum error correction and fault tolerance, *SciPost Physics Lecture Notes*, 070 (2023).
- [8] A. Steane, Multiple-particle interference and quantum error correction, *Proceedings of the Royal Society of London. Series A: Mathematical, Physical and Engineering Sciences* **452**, 2551 (1996).
- [9] A. R. Calderbank and P. W. Shor, Good quantum error-correcting codes exist, *Physical Review A* **54**, 1098 (1996).
- [10] S. B. Bravyi and A. Y. Kitaev, Quantum codes on a lattice with boundary, *arXiv preprint quant-ph/9811052* (1998).
- [11] H. Bombin and M. A. Martin-Delgado, Topological quantum distillation, *Physical review letters* **97**, 180501 (2006).
- [12] A. A. Kovalev and L. P. Pryadko, Quantum kronecker sum-product low-density parity-check codes with finite rate, *Physical Review A* **88**, 012311 (2013).
- [13] S. Bravyi, A. W. Cross, J. M. Gambetta, D. Maslov, P. Rall, and T. J. Yoder, High-threshold and low-overhead fault-tolerant quantum memory, *Nature* **627**, 778 (2024).
- [14] L. Voss, S. J. Xian, T. Haug, and K. Bharti, Trivariate bicycle codes, *arXiv preprint arXiv:2406.19151* [10.48550/arXiv.2406.19151](https://arxiv.org/abs/2406.19151) (2024).
- [15] R. Acharya, L. Aghababaie-Beni, I. Aleiner, T. I. Andersen, M. Ansmann, F. Arute, K. Arya, A. Asfaw, N. Astrakhantsev, J. Atalaya, *et al.*, Quantum error correction below the surface code threshold, *arXiv preprint arXiv:2408.13687* (2024).
- [16] G. Q. AI, Suppressing quantum errors by scaling a surface code logical qubit, *Nature* **614**, 676 (2023).
- [17] D. Bluvstein, S. J. Evered, A. A. Geim, S. H. Li, H. Zhou, T. Manovitz, S. Ebadi, M. Cain, M. Kalinowski, D. Hangleiter, *et al.*, Logical quantum processor based on reconfigurable atom arrays, *Nature* **626**, 58 (2024).
- [18] P. Iyer and D. Poulin, Hardness of decoding quantum stabilizer codes, *IEEE Transactions on Information Theory* **61**, 5209 (2015).
- [19] A. J. Ferris and D. Poulin, Tensor networks and quantum error correction, *Physical review letters* **113**, 030501 (2014).
- [20] C. T. Chubb and S. T. Flammia, Statistical mechanical models for quantum codes with correlated noise, *Annales de l’Institut Henri Poincaré D* **8**, 269 (2021).
- [21] A. Kaufmann and I. Arad, A blockbp decoder for the surface code, *arXiv preprint arXiv:2402.04834* (2024).
- [22] G. Torlai and R. G. Melko, Neural decoder for topological codes, *Physical review letters* **119**, 030501 (2017).
- [23] J. Fujisaki, H. Oshima, S. Sato, and K. Fujii, Practical and scalable decoder for topological quantum error correction with an ising machine, *Physical Review Research* **4**, 043086 (2022).
- [24] Y. Takeuchi, Y. Takada, T. Sakashita, J. Fujisaki, H. Oshima, S. Sato, and K. Fujii, Comparative study of decoding the surface code using simulated annealing under depolarizing noise, *arXiv:2311.07973* (2023).
- [25] Y. Takada, Y. Takeuchi, and K. Fujii, Ising model formulation for highly accurate topological color codes decoding, *Phys. Rev. Res.* **6**, 013092 (2024).
- [26] J. Roffe, D. R. White, S. Burton, and E. Campbell, Decoding across the quantum low-density parity-check code landscape, *Physical Review Research* **2**, 043423 (2020).
- [27] P. Panteleev and G. Kalachev, Degenerate quantum ldpc codes with good finite length performance, *Quantum* **5**, 585 (2021).
- [28] E. Dennis, A. Kitaev, A. Landahl, and J. Preskill, Topological quantum memory, *Journal of Mathematical Physics* **43**, 4452 (2002).
- [29] A. G. Fowler, Minimum weight perfect matching of fault-tolerant topological quantum error correction in average $o(1)$ parallel time, *arXiv preprint arXiv:1307.1740* (2013).
- [30] O. Higgott and C. Gidney, Sparse blossom: correcting a million errors per core second with minimum-weight matching, *arXiv:2303.15933* (2023).
- [31] G. Duclos-Cianci and D. Poulin, Fast decoders for topological quantum codes, *Physical review letters* **104**, 050504 (2010).
- [32] N. Delfosse and N. H. Nickerson, Almost-linear time decoding algorithm for topological codes, *Quantum* **5**, 595 (2021).
- [33] L. Berent, L. Burgholzer, P.-J. H. Derks, J. Eisert, and R. Wille, Decoding quantum color codes with maxsat, *arXiv:2303.14237* (2023).
- [34] I. P. Gent, T. Walsh, and A. Cohn, The sat phase transition (1994) pp. 105–109, *proc European Conference on Artificial Intelligence* 94. John Wiley and Sons.
- [35] V. Chvátal and E. Szemerédi, Many hard examples for resolution, *J. ACM* **35**, 759–768 (1988).
- [36] G. Bresler and B. Huang, The algorithmic phase transition of random k -sat for low degree polynomials (2021), [arXiv:2106.02129 \[cs.CC\]](https://arxiv.org/abs/2106.02129).
- [37] D. Coppersmith, D. Gamarnik, M. Hajiaghayi, and G. B. Sorkin, Random max sat, random max cut, and their phase transitions, *Random Structures & Algorithms* **24**, 502 (2004), <https://onlinelibrary.wiley.com/doi/pdf/10.1002/rsa.20015>.
- [38] J. Berg, M. Jarvisalo, R. Martins, and A. Niskanen, eds.,

- MaxSAT Evaluation 2023: Solver and Benchmark Descriptions*, Department of Computer Science Series of Publications B (Department of Computer Science, University of Helsinki, Finland, 2023).
- [39] S. Bravyi and A. Vargo, Simulation of rare events in quantum error correction, *Physical Review A* **88**, 062308 (2013).
- [40] O. Higgott and N. P. Breuckmann, Improved single-shot decoding of higher-dimensional hypergraph-product codes, *PRX Quantum* **4**, 020332 (2023).
- [41] A. A. Sohangpurwala, M. W. Hassan, and P. Athanas, Hardware accelerated sat solvers—a survey, *Journal of Parallel and Distributed Computing* **106**, 170 (2017).
- [42] C. T. Chubb, General tensor network decoding of 2d pauli codes, arXiv preprint arXiv:2101.04125 (2021).
- [43] H. Bombín and M. A. Martin-Delgado, Optimal resources for topological two-dimensional stabilizer codes: Comparative study, *Physical Review A—Atomic, Molecular, and Optical Physics* **76**, 012305 (2007).
- [44] O. Higgott, Pymatching: A python package for decoding quantum codes with minimum-weight perfect matching, *ACM Transactions on Quantum Computing* **3**, 1 (2022).
- [45] S.-H. Lee, A. Li, and S. D. Bartlett, Color code decoder with improved scaling for correcting circuit-level noise, arXiv preprint arXiv:2404.07482 (2024).
- [46] K. Sahay and B. J. Brown, Decoder for the triangular color code by matching on a möbius strip, *PRX Quantum* **3**, 010310 (2022).
- [47] C. Gidney and C. Jones, New circuits and an open source decoder for the color code, arXiv preprint arXiv:2312.08813 (2023).
- [48] D. S. Wang, A. G. Fowler, C. D. Hill, and L. C. Hollenberg, Graphical algorithms and threshold error rates for the 2d colour code, arXiv preprint arXiv:0907.1708 (2009).
- [49] T. Schubert, M. Lewis, and B. Becker, Pamiraxt: Parallel sat solving with threads and message passing, *Journal on Satisfiability, Boolean Modeling and Computation* **6**, 203 (2010).

Appendix A: Satisfiability Terminology

In Tab. A, we summarise concepts and conventions related to MaxSAT that were used in the paper.

Boolean Variables	In k -SAT, variables can take the values True or False.
Literals	A literal is a variable or its negation. For example, if x_i is a variable, then x_i and $\neg x_i$ (not x_i) are literals.
Clauses	A clause is a disjunction (OR) of literals. In k -SAT, each clause has exactly k literals. For instance, $(x_1 \vee \neg x_2 \vee x_3)$ is a 3-SAT clause.
Conjunctive Normal Form (CNF)	A Boolean formula is in CNF if it is a conjunction (AND) of clauses. For example, $(x_1 \vee x_2 \vee \neg x_3) \wedge (\neg x_1 \vee x_2 \vee x_3)$ is a CNF formula.
Satisfiability	The k -SAT problem asks whether there exists an assignment of True or False to the variables such that the entire CNF formula evaluates to True.

Appendix B: Extended Data

We show the threshold for our MaxSAT decoder and BP-OSD for the Toric code in Fig. 6. We also show also data on more values of distance d on the Color code in Fig. 7.

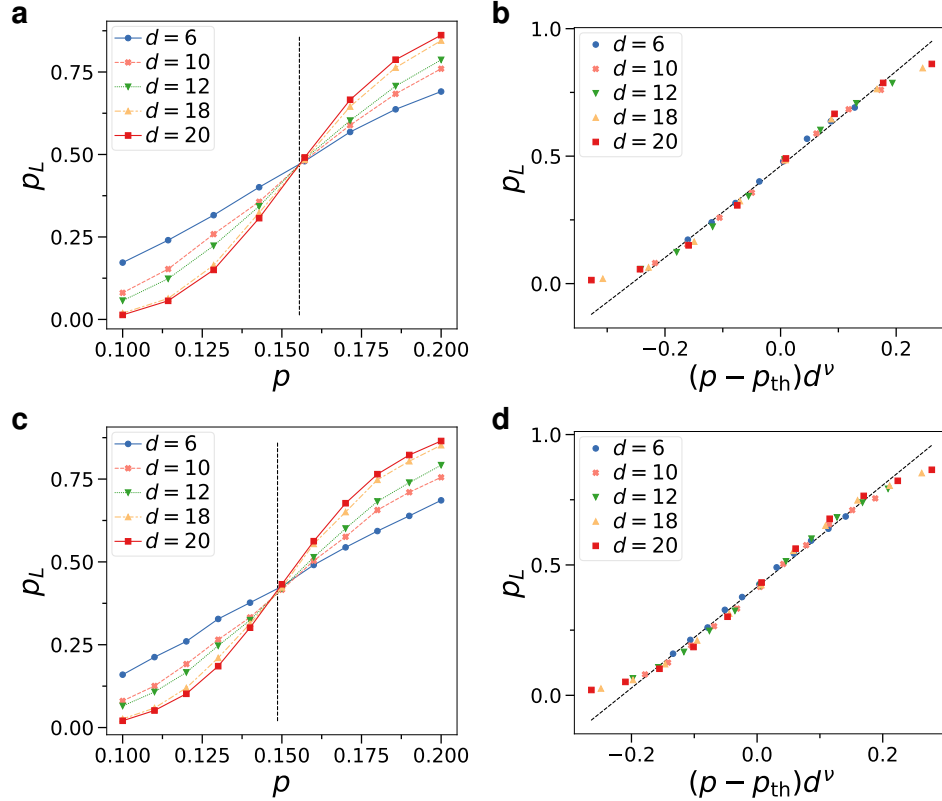


FIG. 6. Threshold for the Toric code using our **a,b** MaxSAT solver and **c,d** BP-OSD. **a,c** We plot logical error rate p_L against physical error rate p for depolarizing noise for different code distances d . We find threshold $p_{th} = 15.55 \pm 0.03\%$ for MaxSAT and $p_{th} = 14.86 \pm 0.03\%$ for BP-OSD. **b,d** Rescaled error plot around p_{th} with exponent $\nu = 0.59$ for MaxSAT and $\nu = 0.56$ BP-OSD, where the dashed line is the fitted critical scaling ansatz.

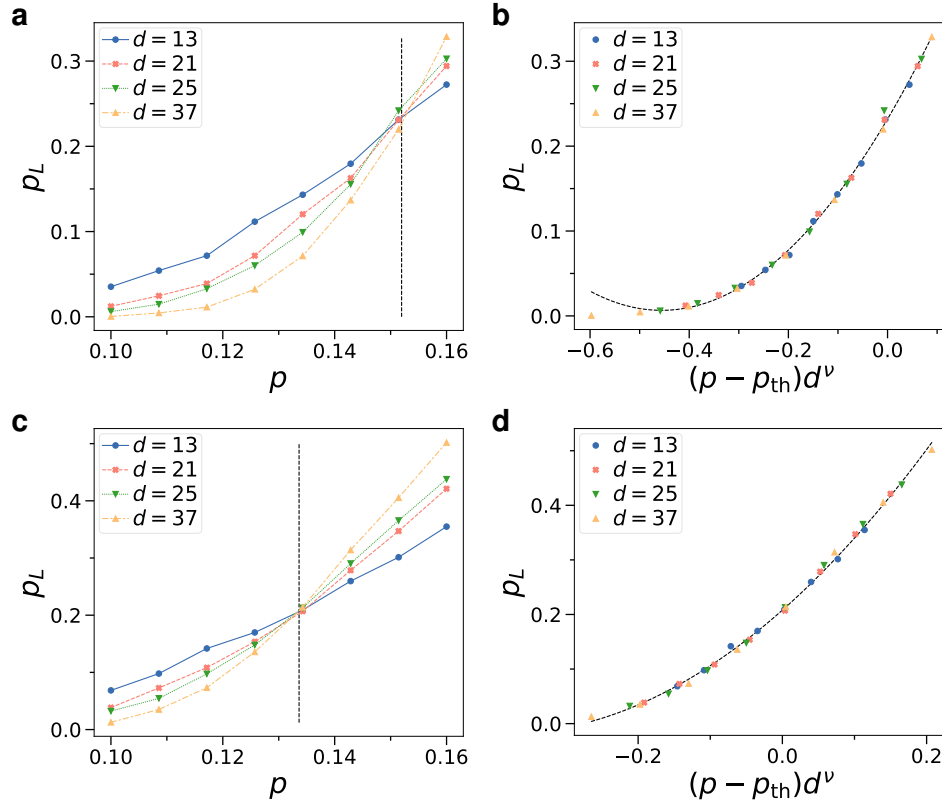


FIG. 7. Threshold for Color code using our **a,b**) MaxSAT solver and **c,d**) BP-OSD. **a,c**) We plot logical error rate p_L against physical error rate p for depolarizing noise for different code distances d . We find threshold $p_{th} = 15.23 \pm 0.05\%$ for MaxSAT and $p_{th} = 13.36 \pm 0.06\%$ for BP-OSD. **b,d**) Rescaled error plot around p_{th} with exponent $\nu = 0.68$ for MaxSAT and $\nu = 0.57$ BP-OSD, where the dashed line is the fitted critical scaling ansatz.